Eksplorium *p*-ISSN 0854-1418
Volume 46 No. 2, June 2025: 386–410 *e*-ISSN 2503-426X

Green Synthesis and Characterization of ZrO_2 Nanoparticles: *In Vitro* Efficacy Against *Echinococcus granulosus* Protoscolices

Mohammad M. Shakir[1]*, Sadia Sh. Hamad[2]

[1] Department of Biology, College of Education for Women, University of Kirkuk, Kirkuk, 36001, Iraq. ORCID: [0000-0002-0359-4161]

[2] Department of Biology, College of Science, University of Kirkuk, Kirkuk, 36001, Iraq.ORCID: [0009-0008-8269-8161]

*Corresponding author: Mohammad M.Shakir Email: mohamadaljuboory@uokirkuk.edu.iq

Article Received: 12 May 2025, Revised: 08 June 2025, Accepted: 18 June 2025

Abstract

Background: Cystic echinococcosis (CE), caused by the parasite *Echinococcus granulosus*, represents a significant global health challenge, necessitating the development of innovative and effective therapeutic strategies. This study aimed, for the first time, to biosynthesize zirconium dioxide nanoparticles (ZrO_2 NPs) via a green route using an aqueous fruit extract of *Tribulus terrestris*, characterize them, and evaluate their *in vitro* scolicidal efficacy against *E. granulosus protoscolices*.

Methods: The synthesized ZrO_2 NPs were comprehensively characterized using X-ray diffraction (XRD), Fourier-transform infrared spectroscopy (FTIR), field emission scanning electron microscopy coupled with energy-dispersive X-ray spectroscopy (FESEM-EDX), zeta potential analysis, and UV-visible spectroscopy (UV-Vis). The scolicidal activity was assessed by exposing protoscolices to various concentrations of ZrO_2 NPs (50–200 µg/mL) for different time intervals (5–60 min). Albendazole (100 µg/mL) and phosphate-buffered saline (PBS) were used as positive and negative controls, respectively.

Results: XRD analysis confirmed the crystalline nature of the ZrO_2 NPs in a cubic fluorite structure with an average crystallite size of ~47.7 nm. FESEM images revealed quasi-spherical particles with a mean diameter of ~48 nm, while FTIR and EDX analyses indicated their successful capping with bioactive compounds from the plant extract. The ZrO_2 NPs exhibited significant concentration- and time-dependent scolicidal activity ($P < 0.001$), with the 200 µg/mL concentration achieving 100% mortality after 60 min. The median lethal concentration (LC_{50}) was 67.8 µg/mL after 60 min. The scolicidal efficacy of ZrO_2 NPs (at ≥150 µg/mL) was significantly higher than that of albendazole ($P < 0.001$).

Conclusion: This study is the first to report the use of *T. terrestris* extract for the biosynthesis of ZrO_2 NPs and to evaluate their scolicidal activity against *E. granulosus*. The results indicate that biosynthesized ZrO_2 NPs possess promising *in vitro* therapeutic potential, positioning them as a viable candidate for developing alternative or adjunctive therapies for CE. Further *in vivo* studies are warranted to assess their clinical efficacy and safety.

Keywords: Cystic echinococcosis, *Echinococcus granulosus*, Zirconium dioxide nanoparticles (ZrO_2 NPs), Green synthesis, Scolicidal activity, *Tribulus terrestris*.

1. INTRODUCTION

Cystic echinococcosis (CE), also known as hydatidosis, is a parasitic zoonosis that poses a significant global burden, with an estimated two to three million people infected annually and substantial economic losses to the livestock industry amounting to billions of dollars (1,2). The disease is caused by infection with the larval stage (hydatid cyst) of the tapeworm *Echinococcus granulosus sensu lato* (s.l.), characterized by the formation of slow-growing, typically unilocular, fluid-filled cysts in vital organs. The liver (~60–70%) and lungs (~20–25%) are the most commonly affected organs, although cysts can also develop in other sites such as the brain, kidneys, spleen, and bones at a lower frequency (3,4). The progression

of these cysts can lead to severe clinical complications, which may be life-threatening in advanced or untreated cases (5 ,6).

However, the current therapeutic management of CE faces considerable challenges due to the limited and variable effectiveness of treatment options. Traditionally, surgical resection of cysts has been the primary treatment, but it is an invasive procedure associated with significant risks, including the spillage of cyst contents containing protoscolices and subsequent disease recurrence (7). Although benzimidazole compounds, primarily albendazole, are used as chemotherapy, either alone or as an adjunct to surgery or minimally invasive techniques like PAIR (Puncture, Aspiration, Injection, Re-aspiration), their efficacy is not optimal. These treatments require long durations, can be accompanied by side effects, and are further complicated by increasing reports of parasite resistance (8,9).

In light of these drawbacks, nanotechnology has emerged as a promising approach for developing innovative strategies against infectious diseases, including parasitic ones. In particular, metallic and metal oxide nanoparticles (MNPs) exhibit unique antimicrobial and antiparasitic properties, primarily attributed to their high surface area-to-volume ratio, which enhances their interaction with biological targets. Their ability to penetrate parasite membranes and cells, and to exert multiple effects on vital biological pathways, such as generating reactive oxygen species (ROS) and inhibiting protein and enzyme functions, is well-documented (10–12). Within this context, zirconium dioxide nanoparticles (ZrO_2 NPs) have garnered increasing research interest due to their distinct physicochemical properties, including high chemical and thermal stability, relatively good biocompatibility, catalytic activity, and reported antioxidant and antimicrobial properties, positioning them for diverse biomedical applications (13–15).

Nevertheless, conventional synthesis methods (chemical and physical) for nanoparticles often involve harsh and toxic chemicals, extreme reaction conditions, high costs, and the generation of environmentally harmful by-products (16,17) . To address these challenges, the green synthesis of nanoparticles has gained significant momentum as a sustainable, cost-effective, and eco-friendly alternative. This approach utilizes biological agents, such as microorganisms or plant extracts rich in bioactive compounds like phenols and flavonoids, as natural reducing and stabilizing (capping) agents (18–20)

Tribulus terrestris L., known for its use in traditional medicine, is a rich source of bioactive compounds such as steroidal saponins and flavonoids, and its extracts have demonstrated a wide range of biological activities, including antiparasitic effects (21,22). In the framework of green synthesis, the role of plant extracts like that of *T. terrestris* is not only limited to facilitating the formation and stabilization of nanoparticles; it is also hypothesized that the plant-derived compounds capping the nanoparticles may contribute synergistically to their therapeutic efficacy (23–25).

Despite the progress in exploring nanoparticles as potential therapeutic agents for CE and considering the promising properties of both ZrO_2 NPs and *T. terrestris* extract, the green synthesis of ZrO_2 NPs using *T. terrestris* extract and the evaluation of their scolicidal activity against *Echinococcus granulosus* represents a largely unexplored research area. Most previous studies have either focused on nanoparticles synthesized by conventional methods or have investigated other types of nanoparticles (e.g., silver, gold, and zinc oxide) against *E.*

granulosus (26–28), with a notable scarcity of research on ZrO_2 NPs, especially those biosynthesized, in this context.

Therefore, to our knowledge, this study aims to achieve, for the first time, the innovative green synthesis of ZrO_2 NPs using an aqueous fruit extract of *T. terrestris* and to perform a preliminary phytochemical analysis of the extract. It also seeks to characterize the physicochemical properties of the synthesized ZrO_2 NPs using advanced techniques. Furthermore, their *in vitro* scolicidal efficacy against *E. granulosus* protoscolices will be evaluated, determining their concentration and time dependency, and comparing it with that of the reference drug, albendazole. It is hypothesized that ZrO_2 NPs synthesized by this method will demonstrate significant scolicidal activity. This work aims to introduce an innovative and eco-friendly approach for developing a potential nanotherapeutic agent against CE, a neglected parasitic disease of global impact. The findings of this study are expected to enrich the scientific understanding of the interactions between biosynthesized nanoparticles and parasites and provide a basis for developing new, more effective, and sustainable therapeutic strategies for this disease.

2. MATERIALS AND METHODS

2.1. Plant Material Sourcing and Authentication

Mature fruits of *Tribulus terrestris* L. were obtained from specialized herbal suppliers in Kirkuk Governorate, Iraq, during August 2024. The plant samples were taxonomically authenticated by a botanist from the Department of Biology, College of Science, University of Kirkuk. A voucher specimen (No KUK-BOT-TT-2024-01) was deposited in the herbarium of the aforementioned department. The fruits were thoroughly washed with distilled water to remove surface contaminants and then air-dried in a well-ventilated, shaded environment at room temperature (25 ± 2 °C) until a constant weight was achieved (approx. 7–10 days), to preserve the stability of their active constituents (Figure 2-1).

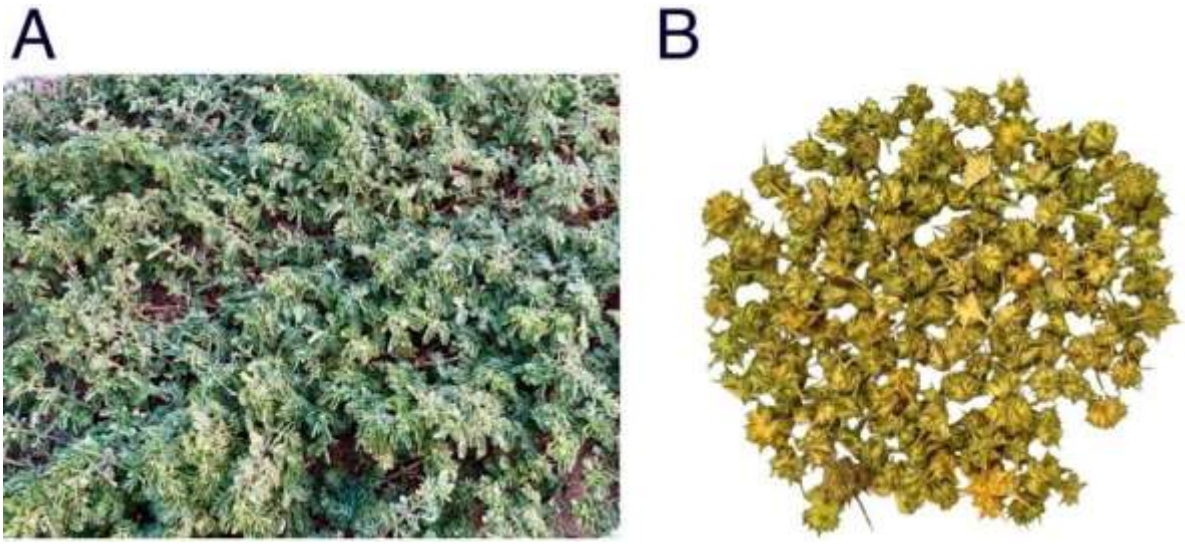

Figure 2-1: Fruits of Tribulus terrestris L. used in the study. (*A*) *General view of the whole T. terrestris L. plant in its habitat.* (*B*) *Dried fruits, after cleaning and drying, served as the raw material for extract preparation.*

2.2. Preparation of *T. terrestris* Dried Aqueous Extract

The dried *T. terrestris* fruits were ground into a fine powder using a laboratory analytical mill (IKA A11 basic, IKA®-Werke GmbH & Co. KG, Staufen, Germany). The resulting powder was sieved through a series of standard-sized sieves (Endecotts Ltd., London, UK) to isolate particles with a size range of [0.5–1 mm].

One hundred grams (100 g) of the sieved powder was subjected to aqueous extraction by maceration in 1000 mL of sterile distilled water (1:10 w/v ratio) in a sterile glass beaker. The mixture was heated to 60 °C and stirred mechanically at 300 rpm for 1 h using a magnetic stirrer with a heating unit (IKA C-MAG HS 7, Staufen, Germany). Subsequently, the mixture was left to steep for 16–18 h (overnight) at room temperature (25 ± 2 °C) to enhance extraction efficiency (29) .

After maceration, the extract was filtered through Whatman No. 1 filter paper (Cytiva, Marlborough, MA, USA) to separate insoluble materials. The filtrate was then centrifuged (4000 rpm, 20 min) in a centrifuge (Eppendorf™ Centrifuge 5810R, Hamburg, Germany) to remove any fine particles. The resulting clear supernatant was collected and completely dried under reduced pressure at 40 °C using a rotary evaporator (BÜCHI™ Rotavapor® R-300, Flawil, Switzerland) to yield a dry aqueous extract powder. The weight of the dry powder was recorded, and it was stored in an airtight container within a desiccator containing silica gel at 4 °C until use.

For the green synthesis of ZrO_2 NPs, a stock solution of the extract was prepared by dissolving a calculated amount of the dry aqueous *T. terrestris* extract powder in double-distilled, deionized water to a final concentration of 100 mg/mL. This reconstituted extract solution was used directly for the nanoparticle synthesis (see Section 2.4).

2.3. Qualitative Phytochemical Screening of *T. terrestris* Extract

A qualitative phytochemical screening of the aqueous *T. terrestris* fruit extract (100 mg/mL) was performed to identify the major groups of secondary metabolites. Standard colorimetric chemical tests were applied, with a particular focus on compounds with potential roles as reducing and stabilizing agents in nanoparticle biosynthesis or those known for their diverse biological activities. The screening primarily included tests for the presence of carbohydrates, alkaloids, phenolic compounds, tannins, flavonoids, saponins, triterpenoids, and steroids, following established protocols described in the literature (30–32) . The presence of resins and cardiac glycosides was also investigated.

2.4. Green Synthesis of Zirconium Dioxide Nanoparticles (ZrO_2 NPs)

Zirconium dioxide nanoparticles (ZrO_2 NPs) were synthesized via a green synthesis method, using the aqueous *T. terrestris* extract (100 mg/mL, as prepared in Section 2.2) as a bioreducing and capping agent. Initially, zirconyl chloride octahydrate ($ZrOCl_2 \cdot 8H_2O$; 3.222 g; [purity ≥99.5%]; [Sigma-Aldrich, St. Louis, MO, USA) was dissolved in 100 mL of deionized water to prepare a 0.1 M precursor solution. This solution was added dropwise to an equal volume of the plant extract (1:1 v/v; 50 mL of each) under continuous magnetic stirring (~500 rpm) at room temperature (25 ± 2 °C). The pH of the reaction mixture was then adjusted to a range of 9.0–10.0 using [1 M] NaOH solution, monitored with a digital pH meter (Hanna Instruments HI2211, Woonsocket, RI, USA) (33,34). The reaction mixture was heated to 60 ±2 °C with

continuous stirring for 3–4 h, during which the formation of a milky-white precipitate was observed. After cooling to room temperature, the precipitate (crude nanoparticles) was separated by centrifugation (8000 rpm, 20 min, 25 ± 2 °C) using a refrigerated centrifuge (Eppendorf 5810R, Hamburg, Germany). The nanoparticles were subjected to repeated washing (5–7 cycles) with deionized water and then absolute ethanol (99.9%), with centrifugation after each wash to remove impurities. The purified product was dried in an air oven (HiMedia AI0049, Kennett Square, PA, USA) at 70 °C for 12–24 h or until constant weight. Finally, the dried powder was calcined in a high-temperature furnace (Kintek KT-14M, Zhengzhou, China) at 650 °C for 3 h and naturally cooled to room temperature to obtain the crystalline phase of ZrO_2 (35,36). The final ZrO_2 NP powder was stored in a desiccator over silica gel until use.

2.5. Characterization of Synthesized ZrO_2 Nanoparticles

A comprehensive characterization of the synthesized and calcined ZrO_2 NPs was conducted to determine their physicochemical properties. X-ray diffraction (XRD; Bruker D8 Advance, Karlsruhe, Germany) was used to identify the crystal structure, phases, average crystallite size, and lattice strain, using a Cu Kα radiation source (λ = 1.5406 Å) over a 2θ range of 10° to 80° (scan step of 0.02°, dwell time of 1 s/step). Fourier-transform infrared spectroscopy (FTIR; Shimadzu IRAffinity-1S, Kyoto, Japan) in the range of 4000–400 cm^{-1} (4 cm^{-1} resolution) was employed to identify surface functional groups, confirm Zr-O bonds, and detect potential plant-derived components involved in capping. Surface morphology, size distribution, and agglomeration degree of the nanoparticles were studied using field emission scanning electron microscopy (FESEM; FEI Nova NanoSEM 450, Hillsboro, OR USA), and the elemental composition was analyzed with purity verification by energy-dispersive X-ray spectroscopy (EDX) coupled to the FESEM. The colloidal dispersion stability and surface charge of the nanoparticles in an aqueous medium (at pH 7.0) were evaluated by measuring the zeta (ζ) potential using a (Malvern Zetasizer Nano ZS, Malvern, UK). Finally, the optical properties and formation of nanoparticles were examined using a UV-visible (UV-Vis) spectrophotometer (Shimadzu UV-1800, Kyoto, Japan) over a wavelength range of 200–800 nm. Samples for each technique were prepared according to standard protocols.

2.6. *In Vitro* Protoscolicidal Assay

2.6.1. Isolation and Purification of *Echinococcus granulosus* Protoscolices

Fertile hydatid cysts of *Echinococcus granulosus* were obtained from the livers and lungs of naturally infected sheep slaughtered at the Kirkuk city abattoir, Iraq, under veterinary supervision. The collected cysts were immediately transported under sterile and refrigerated (4 °C) conditions to the Parasitology Laboratory (Department of Biology, College of Science, University of Kirkuk) for processing within a few hours (Figure 2-2). After sterilizing the cyst surface with 70% (v/v) ethanol, a portion of the hydatid fluid was aspirated with a sterile syringe (23G needle) to reduce internal pressure. The cysts were carefully opened, and their contents, including the fluid and hydatid sand rich in protoscolices, were collected. The suspension was allowed to settle by gravity (30–60 min) at room temperature, and the supernatant was discarded. The protoscolex-containing pellet underwent repeated washing (3–5 cycles) with sterile phosphate-buffered saline (PBS; pH 7.2–7.4), with gentle centrifugation (1500 rpm, 5 min each time). An antibiotic cocktail (penicillin G 100 U/mL and streptomycin

sulfate 100 µg/mL) was added after the second washing cycle to prevent bacterial contamination. The final pellet of purified protoscolices was resuspended in a known volume of PBS, and the suspension was adjusted to a concentration of approximately 5000 viable protoscolices/mL using a Neubauer hemocytometer under microscopic examination.

Figure 2-2: Sheep liver infected with multiple hydatid cysts of Echinococcus granulosus.

2.6.2. Viability Assessment of Protoscolices

The viability percentage of protoscolices was assessed before each experiment by two complementary methods. First, by direct microscopic examination of a drop of the protoscolex suspension (~10 µL) under a light microscope (Olympus CX23, Tokyo, Japan at 100× and 400× magnification), where protoscolices were considered viable upon observation of muscular movements, flame cell activity, or invagination/evagination capabilities. Second, by the eosin vital staining method, where equal volumes (20 µL each) of the protoscolex suspension and 0.1% (w/v) eosin solution in PBS were mixed. After two minutes of incubation at room temperature, the sample was examined microscopically; protoscolices that excluded the dye (remained colorless or pale green) were considered viable, whereas those stained red or pink were considered dead (Figure 2-3). The viability percentage was calculated based on a count of at least 100 protoscolices, and only batches showing an initial viability of ≥97% were used in the experiments.

(Viability formula: Viability (%) = (Number of viable protoscolices / Total number of protoscolices) × 100).

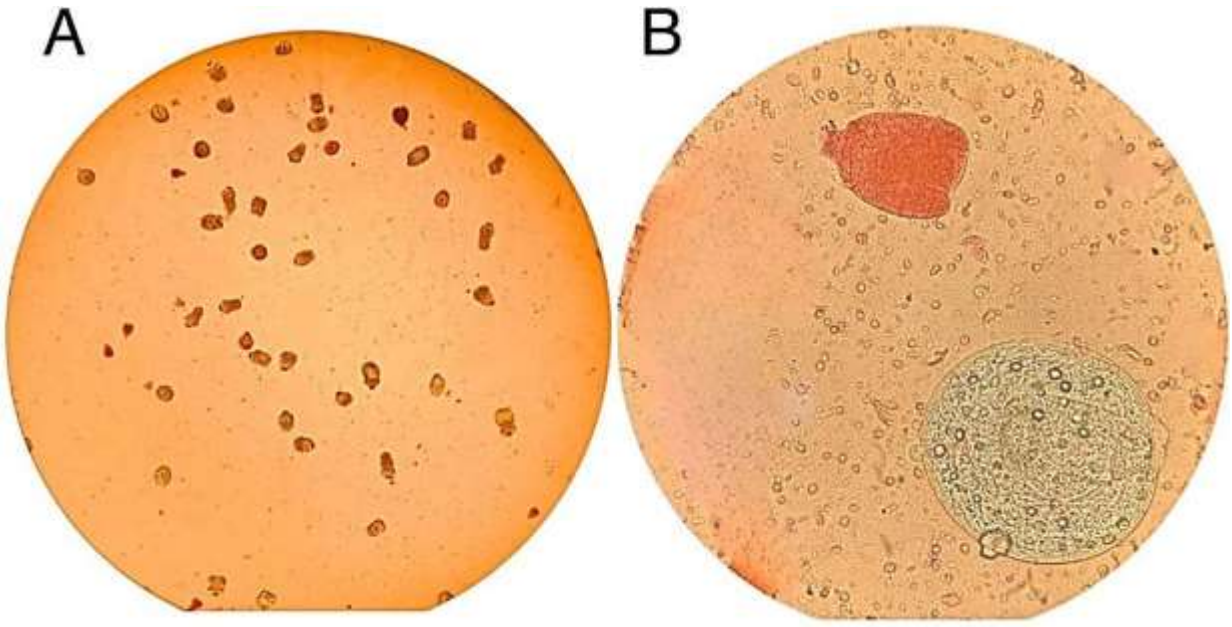

Figure 2-3: Light microscopy images for viability assessment of Echinococcus granulosus protoscolices with 0.1% eosin stain. (A) 100× magnification. (B) 400× magnification, showing viable protoscolices as transparent/pale and dead ones-stained red.

2.6.3. *In Vitro* Scolicidal Activity Assay

The *in vitro* scolicidal activity of the biosynthesized ZrO_2 NPs was evaluated. Different concentrations of ZrO_2 NPs (50, 100, 150, and 200 µg/mL) were prepared by suspending them in sterile PBS (pH 7.2) with sonication for 10 min. One mL of each ZrO_2 NP suspension was added to 1 mL of the protoscolex suspension (containing approx. 5000 viable protoscolices) in sterile glass test tubes (final volume 2 mL) and incubated at 37 ± 0.5 °C. Viability was assessed after exposure times of (5, 10, 15, 30, and 60 min). At each time point, an aliquot (100 µL) was withdrawn, mixed with 0.1% eosin stain, and examined under a microscope to count the number of dead and live protoscolices. Albendazole (purity ≥98%; Sigma-Aldrich, St. Louis, MO, USA) at a concentration of 100 µg/mL (dissolved in a minimal amount of DMSO and then diluted with PBS, such that the final DMSO concentration was <0.5%) was used as a positive control. Sterile PBS alone was used as a negative control. The mortality rate (%) was calculated at each concentration and time point using the formula:

Mortality (%) = (Number of dead protoscolices / Total number of protoscolices examined) × 100. Each experiment was performed in triplicate.

2.7. Statistical Data Analysis

All quantitative data on protoscolex mortality rates were presented as mean ± standard deviation (SD) of three independent replicates. Statistical differences in mortality rates among the different concentrations of ZrO_2 NPs (50, 100, 150, and 200 µg/mL), the control groups, and at the various exposure time points (5, 10, 15, 30, and 60 min) were evaluated using a two-way analysis of variance (ANOVA) with repeated measures. When significant differences were found, Tukey's HSD test was used as a post-hoc multiple comparison test. The median lethal

concentration (LC_{50}) values for each exposure period and the median lethal time (LT_{50}) values for each ZrO_2 NP concentration were estimated using the linear interpolation method. The level of statistical significance was set at a P-value of less than 0.05. All statistical analyses were performed using IBM SPSS Statistics (Version 29.0, IBM Corp., Armonk, NY, USA).

2.8. Ethical Approvals

This study was conducted after obtaining formal approval from the Research Ethics Committee of the Department of Biology, College of Science, University of Kirkuk, Iraq (Approval No: 3/7/2516, Date: 26/3/2024). Hydatid cysts were collected from the livers and lungs of sheep slaughtered for human consumption at the central abattoir in Kirkuk city, under veterinary supervision, ensuring that no animals were sacrificed specifically for this research. All biological samples were handled according to approved biosafety guidelines. The viability of the protoscolices used in the experiments was confirmed to be ≥97% before initiating any activity tests.

3. RESULTS

3.1. Qualitative Phytochemical Screening of *Tribulus terrestris* Extract

The qualitative phytochemical analysis of the aqueous fruit extract of *Tribulus terrestris* revealed the presence of several major classes of secondary metabolites (Table 3-1). The screening tests were positive for carbohydrates, alkaloids (confirmed with both Dragendorff's and Mayer's reagents), phenolic compounds, tannins, flavonoids, saponins, and triterpenoids/steroids (as per the Liebermann-Burchard test). In contrast, tests for resins and cardiac glycosides (Keller-Kiliani test) were negative, indicating their absence or presence at concentrations below the detection limit of the methods used.

Table 3-1: Qualitative phytochemical screening of the major chemical groups in the aqueous fruit extract of Tribulus terrestris.

Phytochemical Group	Chemical Test Used	Observation/Result	Inference*
Carbohydrates	Molisch's test	Formation of a distinct violet ring at the interface.	+
Alkaloids	Dragendorff's test	Formation of an orange-red precipitate.	+
	Mayer's test	Formation of a creamy-white precipitate.	+
Phenolic compounds	Ferric chloride test	Appearance of a dark olive-green color.	+
Tannins	Ferric chloride test	Appearance of a blue-black color.	+
Flavonoids	Shinoda (cyanidin) test	Appearance of a bright crimson-red color.	+
Saponins	Froth test	Formation of a dense and stable foam (>1 cm, lasted >15 min).	+
Triterpenoids and Steroids	Liebermann-Burchard test	Appearance of a bluish-green color, gradually turning brown.	+

Phytochemical Group	Chemical Test Used	Observation/Result	Inference*
Resins	Water precipitation test	No turbidity or white precipitate observed.	-
Cardiac Glycosides	Keller-Kiliani test	No bluish-brown ring or bluish-green color was observed.	-
(+) indicates the presence of the chemical group; (-) indicates its absence or presence at concentrations below the detection limit. *			

3.2. Characterization of Zirconium Dioxide Nanoparticles (ZrO_2 NPs)
3.2.1. X-ray Diffraction (XRD) Analysis

The XRD pattern of the biosynthesized ZrO_2 NPs calcined at 650 °C is presented in Figure 3-1. The pattern displays sharp and well-defined diffraction peaks at 2θ angles of 30.51°, 35.38°, 50.90°, 60.51°, 63.51°, 74.85°, 82.94°, and 85.60°. These peaks correspond to the (111), (200), (220), (311), (222), (400), (331), and (420) crystal planes, respectively, of the cubic fluorite structure of ZrO_2 (JCPDS card No. 96-900-9052). The absence of any additional peaks indicates the high phase purity of the synthesized cubic ZrO_2. The peak corresponding to the (111) plane (2θ ≈ 30.51°) was the most intense. The average crystallite size (D) was estimated to be approximately 47.7 nm using the Debye-Scherrer equation. The lattice constant (a) for the cubic phase was calculated to be 5.070 Å. The Williamson-Hall analysis revealed a low lattice strain (ε) of 0.006–0.009. The calculated theoretical density of the nanoparticles was 6.28 g/cm³, and the unit cell volume was 130.32 Å³.

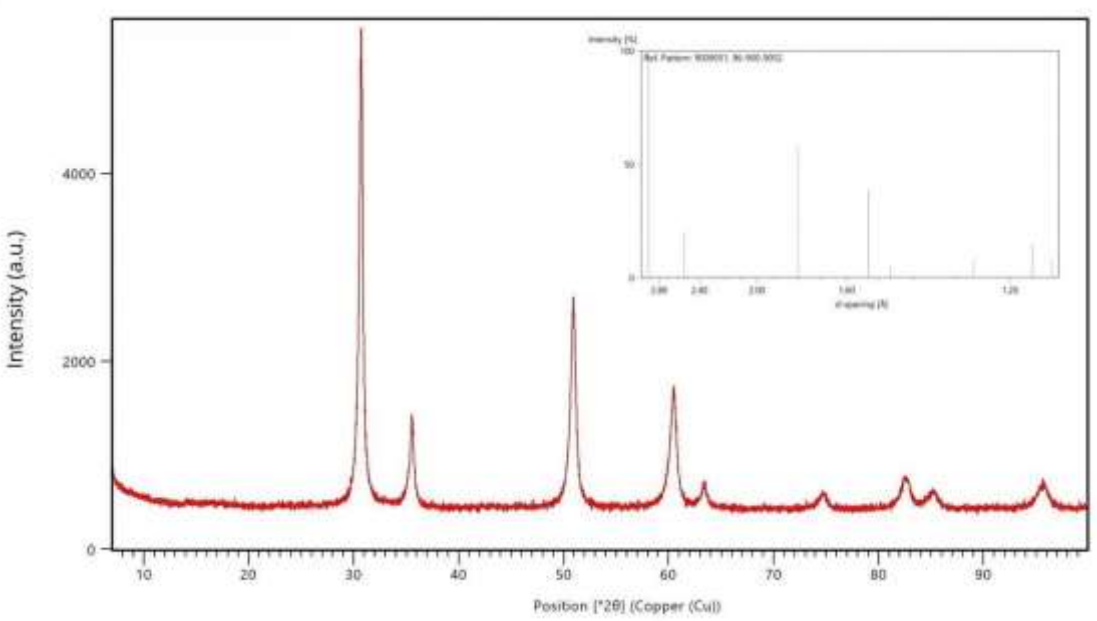

Figure 3-1: X-ray diffraction (XRD) pattern of the biosynthesized ZrO_2 NPs calcined at 650 °C, showing the main diffraction peaks and crystal planes corresponding to the cubic phase.

3.2.2. Fourier-Transform Infrared (FTIR) Spectroscopy

The FTIR absorption spectrum of the biosynthesized ZrO_2 NPs is shown in Figure 3-2. A broad and strong absorption band was observed in the 3000–3600 cm^{-1} region, centered at approximately 3433 cm^{-1}, which is attributed to the stretching vibrations of hydroxyl (O-H) groups. Two distinct peaks appeared at 1051 cm^{-1} and 1007 cm^{-1}, which can be assigned to the stretching vibrations of C-O and possibly C-N bonds from the organic compounds of the plant extract. An absorption peak was also observed at 1620 cm^{-1}, which may arise from the overlapping of H-O-H bending vibrations, C=O stretching vibrations, and/or aromatic C=C vibrations. Critically, the spectrum displayed a sharp and characteristic absorption peak in the fingerprint region at approximately 472 cm^{-1}, which is definitively assigned to the stretching vibrations of the Zr-O metal-oxygen bond in the zirconium oxide lattice.

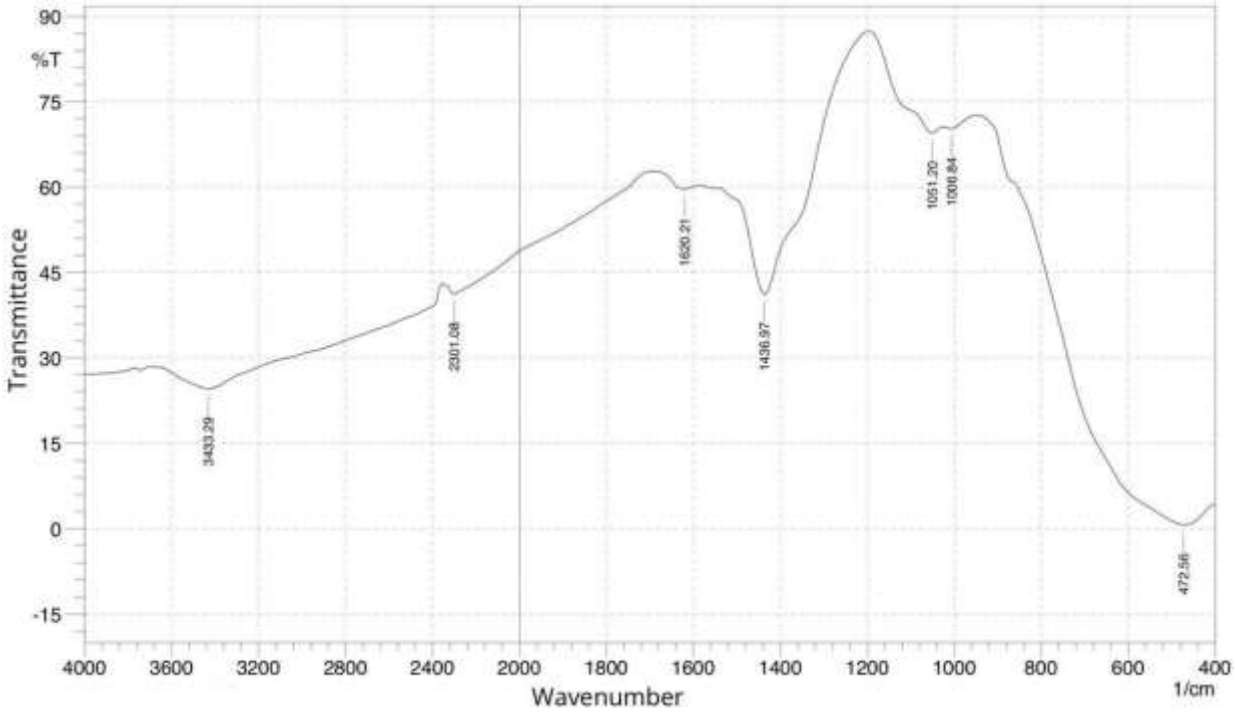

Figure 3-2: Fourier-transform infrared (FTIR) spectrum of ZrO_2 NPs biosynthesized using T. terrestris extract.

3.2.3. Field Emission Scanning Electron Microscopy (FESEM)

FESEM images revealed the morphological characteristics of the synthesized ZrO_2 NPs (Figure 3-3). The particles exhibited a generally quasi-spherical to spherical shape, with a mean diameter of approximately 48 nm. A degree of agglomeration was observed, but individual particles with well-defined boundaries were still distinguishable.

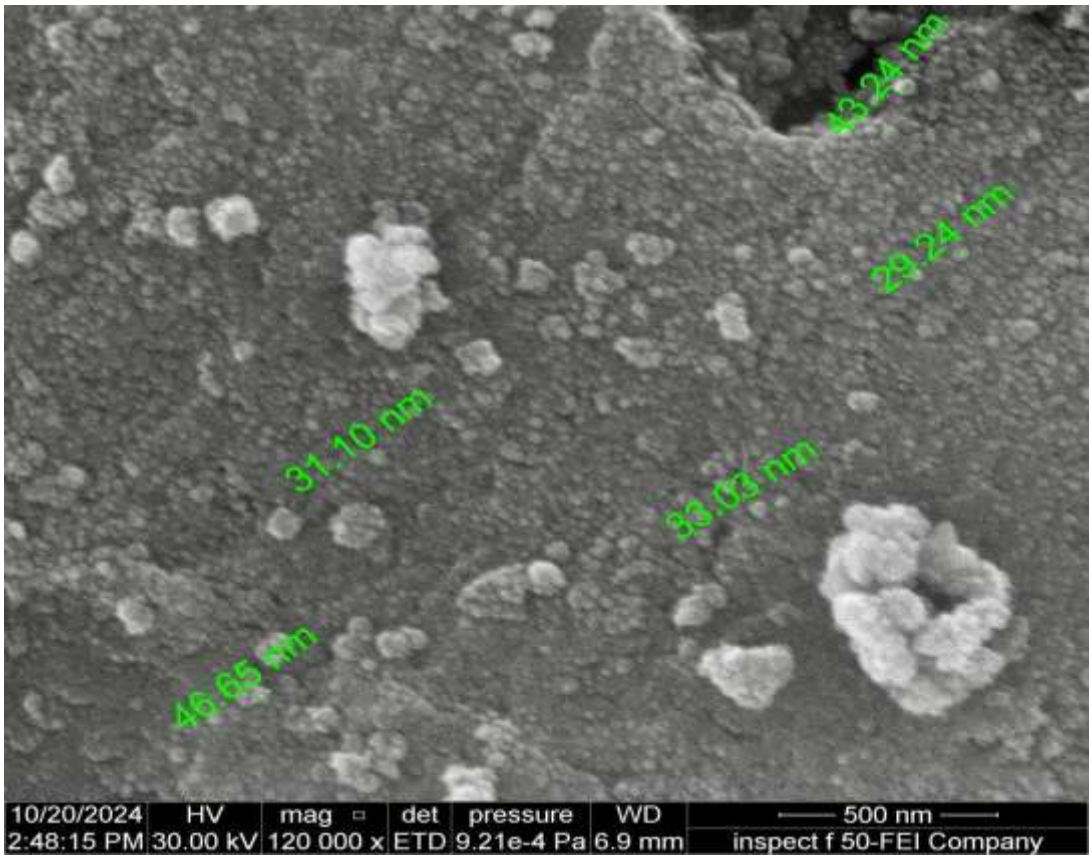

Figure 3-3: Field emission scanning electron microscopy (FESEM) images of the biosynthesized ZrO_2 NPs.

3.2.4. Energy-Dispersive X-ray (EDX) Spectroscopy

EDX analysis confirmed the elemental composition of the ZrO_2 NPs (Figure 3-4 and Table 3-2). The spectrum showed prominent and intense peaks for zirconium (Zr) and oxygen (O). Additionally, the presence of carbon (C) in significant amounts was detected, along with smaller quantities of sodium (Na), calcium (Ca), and nickel (Ni), as detailed in Table 3-2.

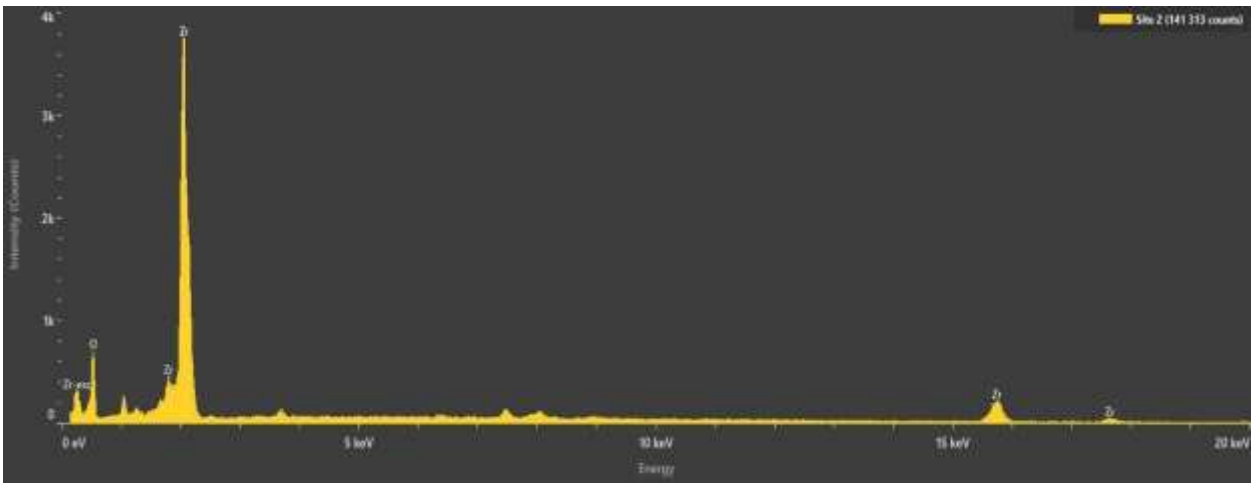

Figure 3-4: A typical energy-dispersive X-ray (EDX) spectrum of the biosynthesized ZrO_2 NPs, showing the characteristic peaks of the detected elements.

Table 3-2: Elemental composition of the biosynthesized ZrO_2 NPs as determined by EDX analysis.

Element	Symbol	Weight %	Atomic %
Carbon	C	14.5 ± 0.4	32.5 ± 1.0
Oxygen	O	28.7 ± 0.6	48.3 ± 1.0
Sodium	Na	2.1 ± 0.1	2.5 ± 0.2
Calcium	Ca	0.6 ± 0.0	0.4 ± 0.0
Nickel	Ni	1.6 ± 0.2	0.8 ± 0.1
Zirconium	Zr	52.4 ± 1.8	15.5 ± 0.5

3.2.5. Zeta Potential Measurement

Zeta potential measurements of the biosynthesized ZrO_2 NPs suspended in deionized water (at pH 7.0) showed a mean value of -41.86 mV (Figure 3-5).

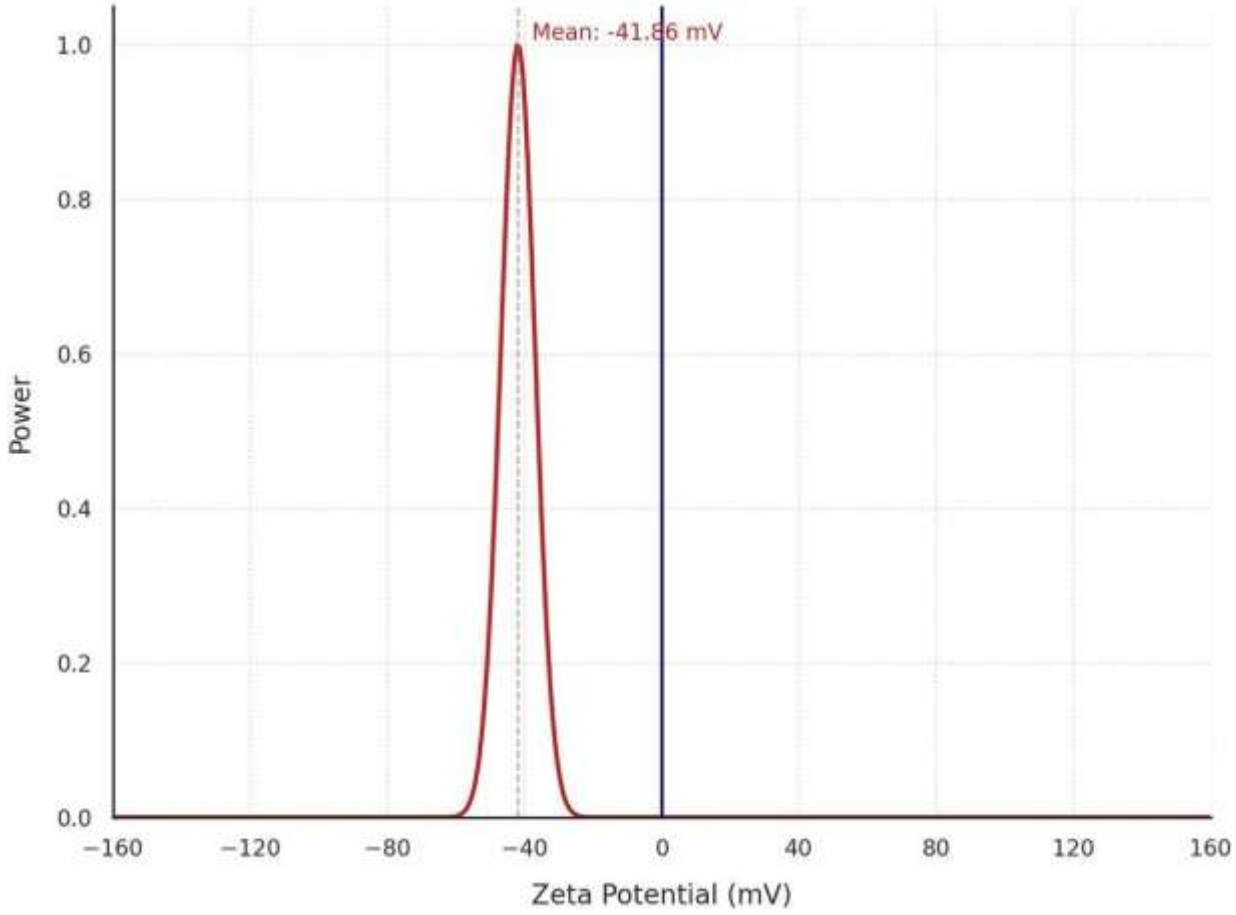

Figure 3-5: Zeta potential distribution curve of the biosynthesized ZrO_2 NP suspension, showing the average zeta potential value.

3.2.6. UV-Visible (UV-Vis) Spectroscopy

The UV-Vis absorption spectrum of the biosynthesized ZrO_2 NP suspension (Figure 3-6) showed a characteristic absorption in the UV region, with a main absorption peak at approximately 221.5 nm and a distinct shoulder at around 208.5 nm.

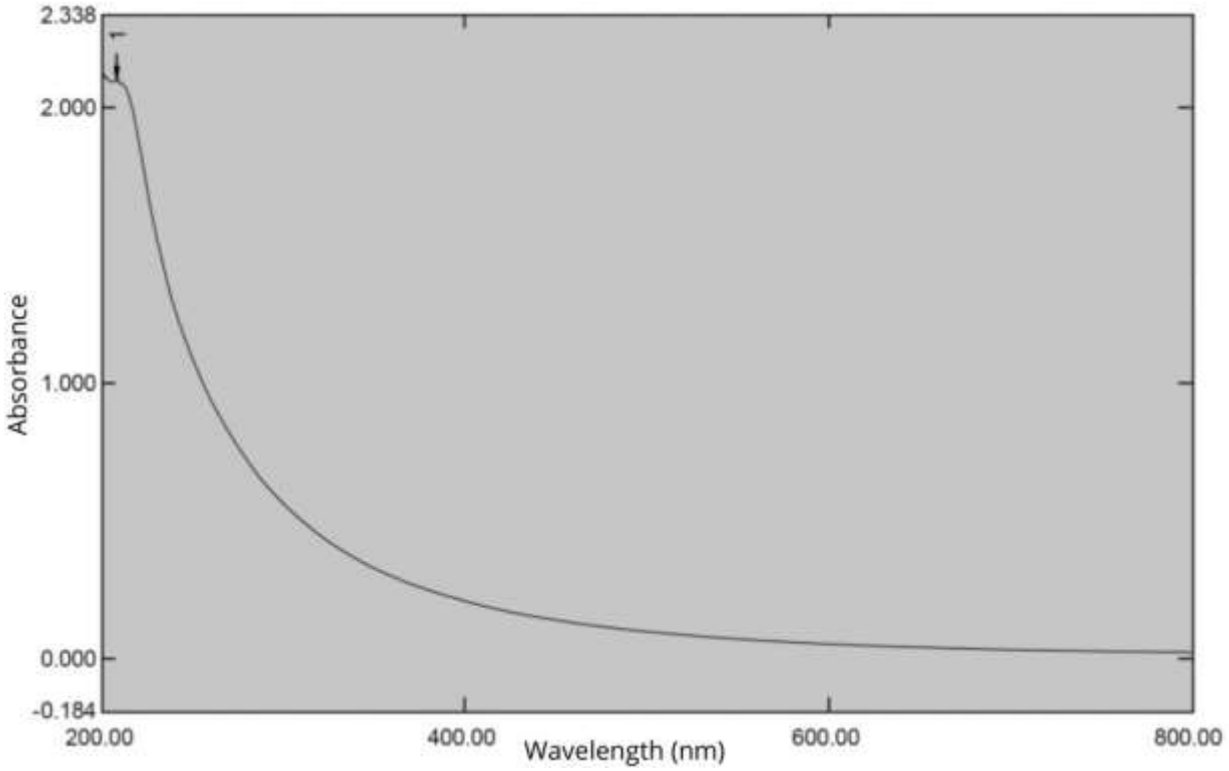

Figure 3-6: UV-visible (UV-Vis) absorption spectrum of the biosynthesized ZrO_2 NP suspension.

3.3. *In Vitro* Scolicidal Activity of ZrO_2 Nanoparticles

3.3.1. Morphological Alterations in Protoscolices

Light microscopy revealed marked morphological alterations in *E. granulosus* protoscolices after exposure to ZrO_2 NPs, compared to the negative control group (PBS), which maintained its normal structure and viability (Figure 3-7A, B). Protoscolices treated with ZrO_2 NPs (e.g., at 200 µg/mL for 60 min) showed a complete loss of motility, body shrinkage and deformity, scolex invagination, cytoplasmic vacuolization, deterioration of the tegument integrity with the formation of blebs, and disturbance and loss of hooks (Figure 3-7C-F).

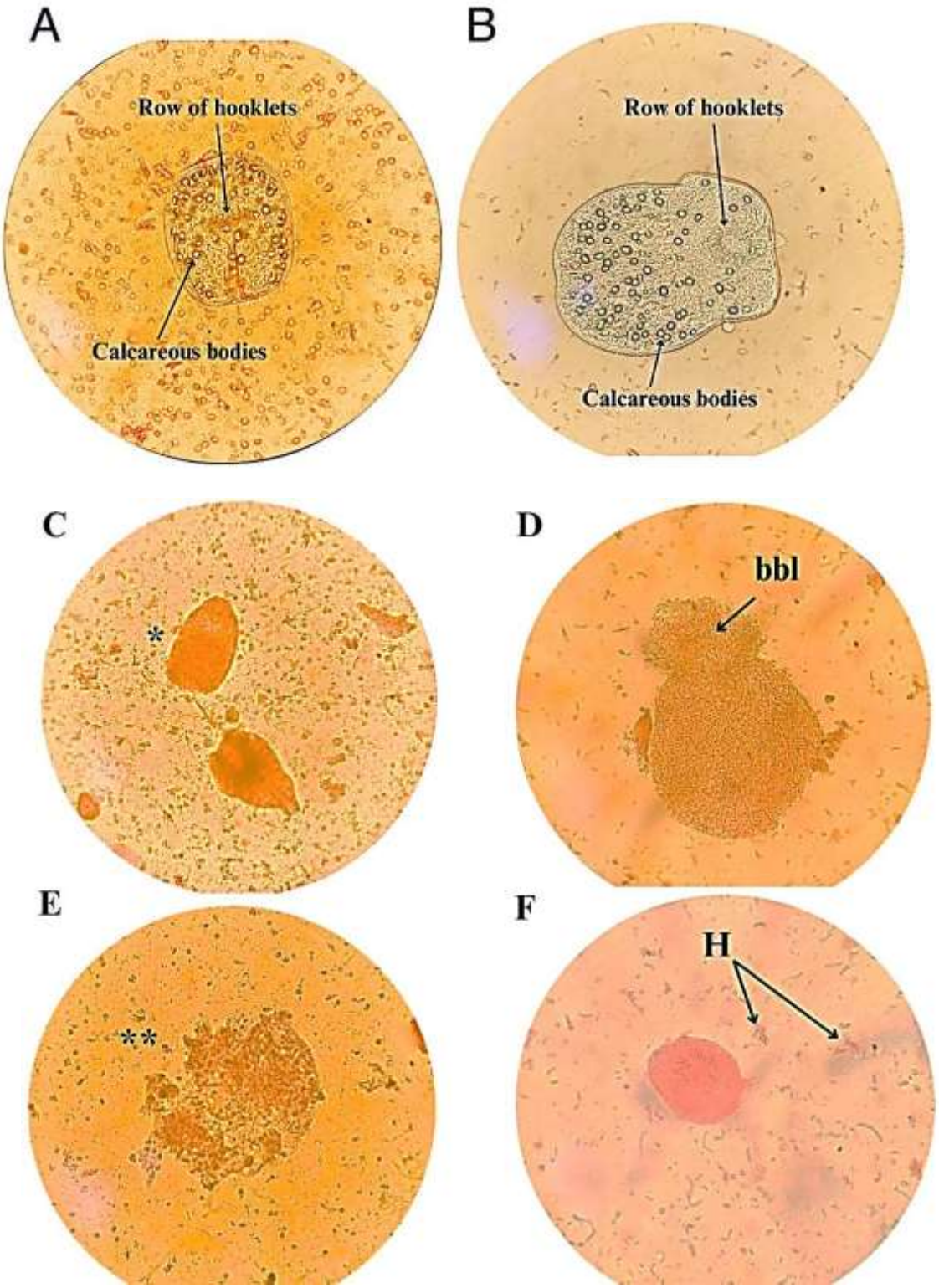

Figure 3-7: Morphological alterations in E. granulosus protoscolices under light microscopy (400×). (A, B) Protoscolices from the control group (PBS), showing viability and normal structure (A: invaginated, B: evaginated with clear scolex and hooks). (C–F) Protoscolices treated with 200 µg/mL of ZrO_2 NPs after 60 min, showing: (C) shrinkage and scolex invagination (*), (D) tegumental deterioration and bleb formation (bbl), (E) tissue disintegration and scattered calcareous corpuscles (**), (F) loss and scattering of hooks (H).

3.3.2. Concentration- and Time-Dependent Efficacy

The results showed that the biosynthesized ZrO_2 NPs possessed a clear scolicidal activity against *Echinococcus granulosus* protoscolices in a concentration- and time-dependent manner (Figure 3-8 and Table 3-3). Correlation analysis revealed a very strong and significant positive relationship between increasing concentration and increasing scolicidal efficacy ($r = 0.967$, $P < 0.001$). At a low concentration (50 µg/mL), the scolicidal effect started at 8.7 ± 0.4% after 5 min and gradually increased to 69.8 ± 0.7% after 60 min. As the concentration was increased to 100 µg/mL, the scolicidal efficacy was markedly enhanced, reaching 18.8 ± 0.7% and 85.3 ± 0.6% after 5 and 60 min, respectively. The two highest concentrations (150 and 200 µg/mL) showed outstanding efficacy; the 150 µg/mL concentration achieved a mortality rate of 99.7 ± 0.2% after 60 min, while the 200 µg/mL concentration achieved complete mortality (100.0 ± 0.0%) within the same period.

Compared to albendazole (100 µg/mL) as a positive control, which showed a mortality rate of 89.7 ± 0.6% after 60 min, the ZrO_2 NPs at high concentrations (150 and 200 µg/mL) demonstrated similar or superior efficacy. The negative control group (PBS) showed a very low natural mortality rate that did not exceed 1.2 ± 0.2% even after 60 min. As detailed in Table 3-3, a two-way ANOVA confirmed that the scolicidal effect was significantly dependent on both concentration and exposure time, with a significant interaction between these two factors ($P < 0.001$ for all).

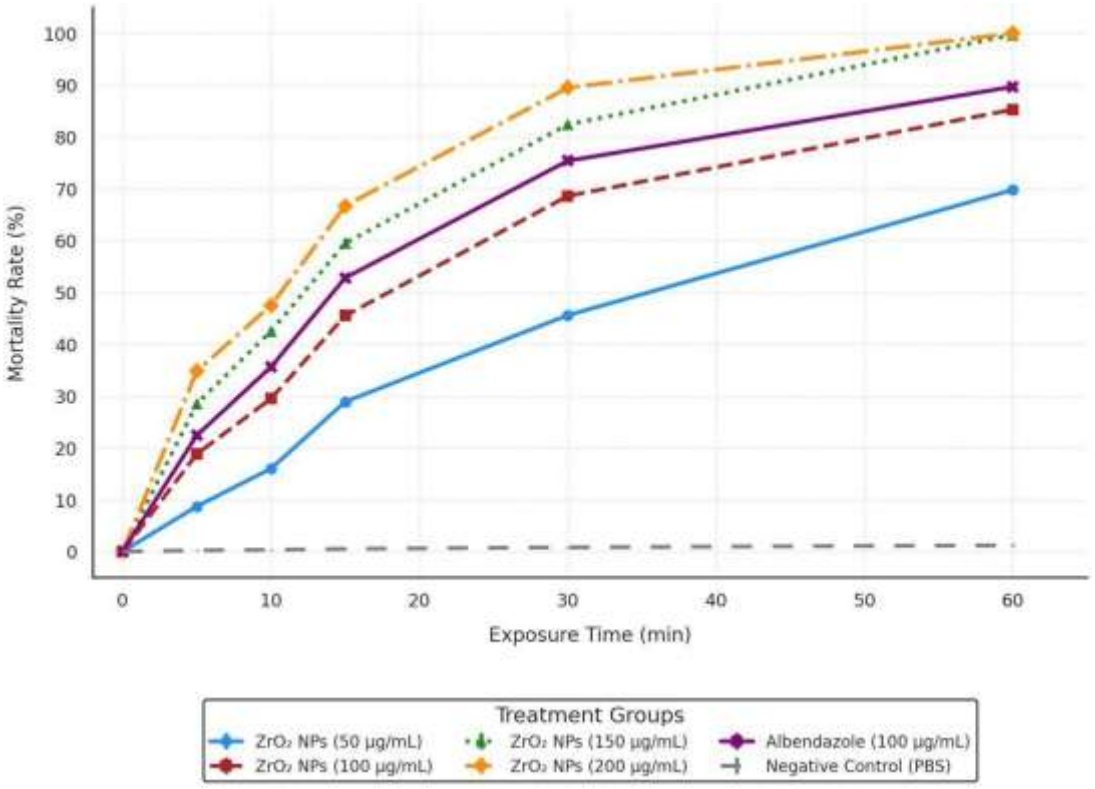

Figure 3-8: Mortality percentage of E. granulosus protoscolices after exposure to different concentrations of ZrO_2 NPs (50–200 µg/mL), albendazole (100 µg/mL), and the control group (PBS) for increasing time intervals (5, 10, 15, 30, and 60 min). Data are presented as mean ± SD (n=3).

Table 3-3: Mean mortality percentage ± standard deviation (SD) of E. granulosus protoscolices after exposure to different concentrations of ZrO_2 NPs and albendazole.

Treatment (Concentration, µg/mL)	5 min	10 min	15 min	30 min	60 min
ZrO_2 NPs (50)	8.7 ± 0.4e, A	16.0 ± 0.3e, B	28.9 ± 0.6d, C	45.6 ± 0.6d, D	69.8 ± 0.7c, E
ZrO_2 NPs (100)	18.8 ± 0.7d, A	29.5 ± 0.6d, B	45.5 ± 0.7c, C	68.6 ± 1.0c, D	85.3 ± 0.6b, E
ZrO_2 NPs (150)	28.5 ± 0.7c, A	42.5 ± 0.7c, B	59.5 ± 0.9b, C	82.4 ± 0.7b, D	99.7 ± 0.2a, E
ZrO_2 NPs (200)	34.8 ± 0.9b, A	47.5 ± 0.8b, B	66.7 ± 1.2a, C	89.5 ± 0.7a, D	100.0 ± 0.0a, E
Albendazole (100)	22.4 ± 0.7cd, A	35.6 ± 0.6cd, B	52.8 ± 0.7bc, C	75.4 ± 0.7b, D	89.7 ± 0.6b, E
PBS (Negative Control)	0.2 ± 0.1f, A	0.3 ± 0.1f, A	0.5 ± 0.1e, A	0.8 ± 0.1e, A	1.2 ± 0.2d, A

Values represent the mean of three replicates ± standard deviation (SD). Different lowercase letters (a,b,c,d,e,f) within the same column indicate statistically significant differences ($P < 0.05$) among different concentrations at the same time point, according to Tukey's test. Different uppercase letters (A, B, C, D, E) within the same row indicate statistically significant differences ($P < 0.05$) among different exposure periods for the same concentration, according to Tukey's test. A two-way ANOVA confirmed a significant main effect for concentration ($F(5, 12) = 892.45$, $P < 0.001$, $\eta^2 = 0.897$), time ($F(4, 48) = 1245.67$, $P < 0.001$, $\eta^2 = 0.912$), and a
significant concentration-time interaction ($F(20, 48) = 124.89$, $P < 0.001$, $\eta^2 = 0.839$).

3.3.3. Median Lethal Concentration (LC_{50}) and Median Lethal Time (LT_{50}) Values

The calculated results using the linear interpolation method revealed a clear and gradual decrease in the median lethal concentration (LC_{50}) values with increasing exposure time (Table 3-4 and Figure 3-9a). At short time intervals (5 and 10 min), the LC_{50} values exceeded the tested range (>200 µg/mL). The LC_{50} values began to decrease substantially at 15 min to 116.07 µg/mL, further dropping to 59.57 µg/mL at 30 min and falling below the lowest tested concentration (<50 µg/mL) after 60 min of exposure.

Conversely, the median lethal time (LT_{50}) values showed a strong inverse relationship with the applied concentration (Table 3-4 and Figure 3-9b). At the low concentration (50 µg/mL), the protoscolices required 35.45 min to reach 50% mortality, whereas this duration decreased significantly with increasing concentration to 17.92 min (at 100 µg/mL), 12.21 min (at 150 µg/mL), and 10.65 min (at 200 µg/mL).

Table 3-4: Median lethal concentration (LC_{50}) and median lethal time (LT_{50}) values of ZrO_2 NPs against Echinococcus granulosus protoscolices

Parameter	Value
Median Lethal Concentration (LC_{50}) at Different Exposure Periods	
5 min	> 200 µg/mL
10 min	> 200 µg/mL
15 min	116.07 µg/mL
30 min	59.57 µg/mL
60 min	< 50 µg/mL
Median Lethal Time (LT_{50}) at Different Concentrations	
50 µg/mL	35.45 min
100 µg/mL	17.92 min
150 µg/mL	12.21 min
200 µg/mL	10.65 min

All values were calculated using the linear interpolation method.

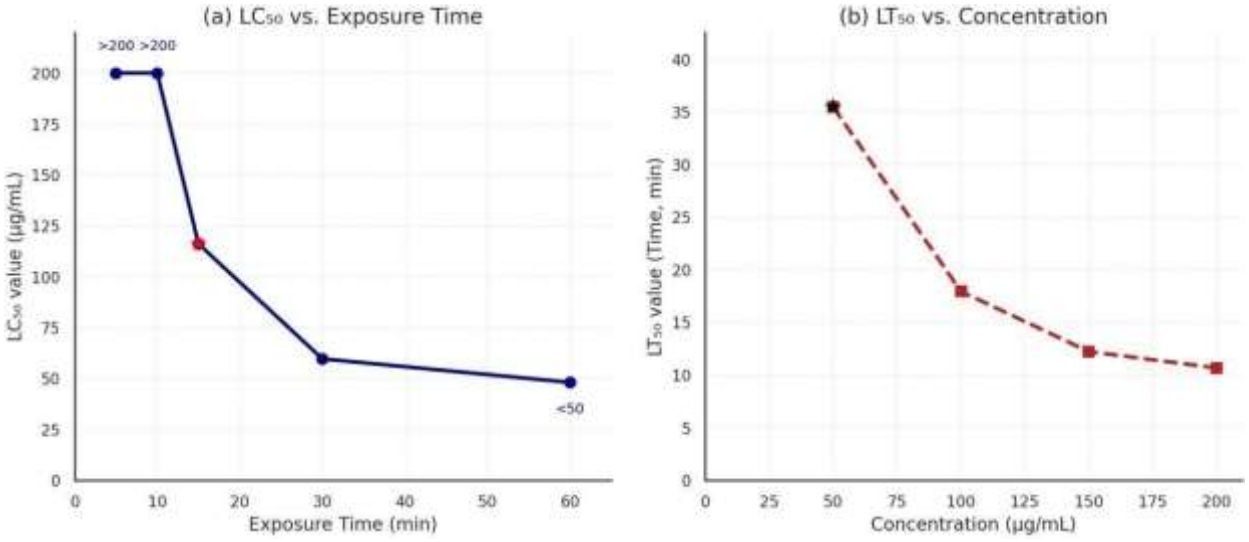

Figure 3-9: Median lethal concentration (LC_{50}) and median lethal time (LT_{50}) values of biosynthesized ZrO_2 NPs against E. granulosus protoscolices. (a) LC_{50} values (µg/mL) versus exposure time (min). LC_{50} values exceeding 200 µg/mL (at 5 and 10 min) or below 50 µg/mL (at 60 min) are indicated by text annotations. The red star highlights the LC_{50} at 15 min. (b) LT_{50} values (min) versus ZrO_2 NP concentration (µg/mL). The black star highlights the LT_{50} at a concentration of 50 µg/mL. Values were calculated by linear interpolation.

4. DISCUSSION

The present study successfully demonstrated the innovative green synthesis of zirconium dioxide nanoparticles (ZrO_2 NPs) using an aqueous fruit extract of *Tribulus terrestris*, followed by their comprehensive characterization and evaluation of their scolicidal efficacy against *Echinococcus granulosus in vitro*. The qualitative phytochemical screening of the *T. terrestris* extract (Table 3-1) revealed a rich profile of major secondary metabolite groups, including carbohydrates, alkaloids, phenolic compounds, tannins, flavonoids, saponins, triterpenoids, and steroids. This phytochemical profile is consistent with the known composition of *T. terrestris*, a plant renowned for its use in traditional medicine and its diverse pharmacological properties, which include antioxidant, antimicrobial, and antiparasitic activities attributed to many of these compounds (25,37–41). The presence of this complex mixture of bioactive molecules, particularly those containing functional groups such as hydroxyl, carbonyl, and amine, is believed to be responsible for the extract's ability to act as an effective reducing agent for zirconium ions and as a stabilizing and capping agent for the resulting nanoparticles (23,24,42–44). The absence of resins and cardiac glycosides, as indicated by the Keller-Kiliani test, may be attributed to their naturally low concentrations in the plant or the limited efficiency of aqueous extraction for these specific compounds (45).

The results of the physicochemical characterization confirmed the successful green synthesis of ZrO_2 NPs. The XRD analysis (Figure 3-1) showed a well-defined crystalline pattern corresponding to the pure cubic fluorite structure of ZrO_2, with an average crystallite size estimated at ~47.7 nm. The stabilization of this cubic phase at a calcination temperature of 650 °C is a significant finding, as it typically requires harsher conditions or the presence of ionic stabilizers (14,46). This stability can be explained by the small nanosize effect and/or the potential role of organic compounds from the plant extract as structural stabilizers (47). The low lattice strain calculated from the Williamson-Hall analysis indicated a good degree of crystallinity and a stable lattice structure.

FTIR spectroscopy results (Figure 3-2) supported these observations and confirmed the hybrid nature of the nanoparticles. A characteristic absorption band for the Zr-O bond (at ~472 cm^{-1}) confirmed the formation of zirconium oxide. Additionally, the spectra revealed the presence of functional groups (e.g., O-H, C-O, C=O) attributed to phenolic, alcoholic, and other compounds from the plant extract. This strongly suggests that the nanoparticle surface was capped by these bioactive molecules, which is consistent with the principles of green synthesis and the role of the extract as a capping agent (20).

FESEM images (Figure 3-3) showed quasi-spherical nanoparticles with a mean diameter of ~48 nm, which is in good agreement with the crystallite size calculated from XRD. Although some agglomeration was observed, a common phenomenon for nanopowders, individual particles were well-defined. EDX analysis (Figure 3-4 and Table 3-2) further substantiated these findings by confirming the primary elemental composition (Zr and O) and showing a significant carbon signal, which also supports the hypothesis of organic capping from the plant extract (48–50). The other elements detected in trace amounts (Na, Ca, Ni) are likely minor impurities from the precursor materials or trace components of the extract.

The high negative zeta potential value (-41.86 mV) (Figure 3-5) indicated good electrostatic stability of the nanoparticle suspensions in an aqueous medium. This negative surface charge

is typically attributed to the ionization of acidic functional groups (such as carboxyl or phenolic hydroxyl groups) from the plant-derived capping agents, leading to repulsion between particles and preventing agglomeration (34,35). Finally, the UV-Vis spectrum (Figure 3-6) showed a characteristic absorption in the UV region (a peak at ~221.5 nm and a shoulder at ~208.5 nm), reflecting the unique electronic and optical properties of the nano-sized ZrO_2. These properties can be influenced by particle size and the surface capping by organic compounds (51).

In this study, the biosynthesized ZrO_2 NPs demonstrated a remarkable scolicidal activity against *E. granulosus* protoscolices *in vitro*, with the effect being highly dependent on both nanoparticle concentration and exposure time (Figure 3-8, Tables 3-3 and 3-4). These findings are consistent with the growing trend of exploring various nanomaterials as scolicidal agents (26,52–54). The achievement of 100% protoscolex mortality at a concentration of 200 µg/mL after 60 min, and the significantly superior efficacy of ZrO_2 NPs at concentrations of 150 and 200 µg/mL compared to the reference drug albendazole (100 µg/mL) over the same period, are strong indicators of the therapeutic potential of these nanoparticles. This high efficiency is further supported by the LC_{50} values, which decreased markedly with increasing exposure time, and the short LT_{50} values at higher concentrations (Table 3-4, Figure 3-9).

The severe morphological alterations observed in the treated protoscolices (Figure 3-7), such as body shrinkage, tegumental integrity loss, and hook detachment, suggest multiple and destructive mechanisms of action. This high efficacy can be attributed to a combination of synergistic factors. First, the physical properties of the nanoparticles, such as their small size (~48 nm) and increased reactive surface area, may facilitate their penetration of the parasite's membranes and interaction with its biological components (34,55). Second, ZrO_2 NPs themselves may possess catalytic activity or intrinsic toxicity, such as the ability to generate reactive oxygen species (ROS) that cause lethal oxidative stress in the parasite cells (56,57). Third, it is highly probable that the plant-derived compounds from the *T. terrestris* extract capping the nanoparticle surface contribute to the overall efficacy. Many of these compounds (e.g., phenolics, flavonoids, saponins, and alkaloids) possess intrinsic antiparasitic properties and may act synergistically with the ZrO_2 core to enhance the scolicidal effect (20,58–60).

The use of *T. terrestris* extract for the green synthesis of ZrO_2 NPs represents a promising and eco-friendly approach that avoids many of the drawbacks of conventional nanoparticle manufacturing methods and may enhance their biocompatibility and therapeutic efficacy (25,38–40,65). However, despite the positive *in vitro* results of this study, it is essential to acknowledge its limitations and look toward future research to translate these findings into potential clinical applications. The present study is confined to laboratory evaluation; the precise molecular mechanisms of action have not been fully elucidated, and the toxicity of these nanoparticles on host cells or *in vivo* models has not been assessed. Therefore, future research priorities should include evaluating the *in vivo* efficacy in infected animal models, conducting comprehensive cellular and systemic toxicity studies to determine the safety profile of these nanoparticles, and further exploring their antiparasitic mechanisms of action at the molecular level. Additionally, studying the pharmacokinetics and biodistribution of the nanoparticles, and potentially improving their pharmaceutical formulation and developing targeted delivery systems for hydatid cysts, are important future directions.

5. CONCLUSIONS

This study successfully demonstrated the effective green synthesis of zirconium dioxide nanoparticles (ZrO_2 NPs) using an aqueous fruit extract of *Tribulus terrestris*. The synthesized nanoparticles were characterized by desirable physicochemical properties, including a pure cubic crystalline phase, a nanosized dimension (mean diameter ~48 nm), surface capping by plant-derived compounds, and good stability in aqueous suspension.

The biosynthesized ZrO_2 NPs exhibited concentration- and time-dependent scolicidal activity against *Echinococcus granulosus* protoscolices *in vitro*. A concentration of 200 µg/mL resulted in 100% mortality of protoscolices after 60 minutes, and the nanoparticles were significantly more effective than the reference drug albendazole at concentrations of 150 and 200 µg/mL. The low median lethal concentration (LC_{50}) of 67.8 µg/mL after 60 minutes and the short median lethal times (LT_{50}) at higher concentrations supported this efficacy.

These findings strongly support the hypothesis that ZrO_2 NPs biosynthesized using *T. terrestris* extract possess promising potential as a scolicidal agent against *E. granulosus*. Consequently, these nanoparticles can be considered a viable candidate for the development of new or adjunctive therapeutic strategies for cystic echinococcosis.

This study highlights the importance of utilizing green nanotechnology and natural resources to develop innovative solutions for neglected parasitic diseases. However, further *in vivo* studies are strongly recommended to evaluate the clinical efficacy and biosafety of these nanoparticles, as well as a deeper exploration of their molecular mechanisms of action, before any future clinical applications can be considered.

DECLARATION OF COMPETING INTERESTS

The authors declare that they have no known competing financial interests or personal relationships that could have appeared to influence the work reported in this paper.

REFERENCES

1. Hogea MO, Ciomaga BF, Muntean MM, Muntean AA, Popa MI, Popa GL. Cystic Echinococcosis in the Early 2020s: A Review. Trop Med Infect Dis. 2024 Jan 31;9(2):36.
2. Bekele T, Fentaw N, Teshale A, Mosu S. Prevalence of Hydatidosis in Cattle Slaughtered at Bishoftu Municipal Abattoir, Ethiopia, and Assessment of Its Economic Loss and Community Awareness. Vet Med Int. 2024 Jan 22;2024(1).
3. Woolsey ID, Miller AL. Echinococcus granulosus sensu lato and Echinococcus multilocularis: A review. Res Vet Sci. 2021 Mar;135:517–22.
4. Aziz H, Seda P, Aswani Y, Gosse MD, Krishnakumari AJ, Pawlik TM. Cystic echinococcosis of the liver. Journal of Gastrointestinal Surgery. 2025 Mar;29(3):101974.
5. Santucciu C, Bonelli P, Peruzzu A, Fancellu A, Marras V, Carta A, et al. Cystic echinococcosis: Clinical, immunological, and biomolecular evaluation of patients from Sardinia (Italy). Pathogens. 2020 Nov 1;9(11):1–18.
6. Baruah A, Sarma K, Barman B, Phukan P, Nath C, Boruah P, et al. Clinical and Laboratory Presentation of Hydatid Disease: A Study From Northeast India. Cureus. 2020 Sep 5;

7. Shakir MM, Hassan HF. Epidemological and Parasitological Studies on Hydatidosis in Kirkuk Province, Iraq. Vol. 13. 2018.

8. Bakhtiar NM, Akbarzadeh A, Casulli A, Mahami-Oskouei M, Ahmadpour E, Nami S, et al. Therapeutic efficacy of nanocompounds in the treatment of cystic and alveolar echinococcoses: challenges and future prospects. Vol. 118, Parasitology Research. Springer Verlag; 2019. p. 2455–66.

9. Sadr S, Lotfalizadeh N, Abbasi AM, Soleymani N, Hajjafari A, Roohbaksh Amooli Moghadam E, et al. Challenges and Prospective of Enhancing Hydatid Cyst Chemotherapy by Nanotechnology and the Future of Nanobiosensors for Diagnosis. Vol. 8, Tropical Medicine and Infectious Disease. Multidisciplinary Digital Publishing Institute (MDPI); 2023.

10. Hamad SS, Abdulla HM, Al-Aubaidi IK. Epidemiological Study of Toxoplasmosis in Patients with Renal Failure form Kirkuk City /Iraq [Internet]. Available from: www.jgpt.co.in

11. Yousif FH, Mohammed SH, Ali MJ. The Antimicrobial Effect of Silver Nanoparticles on some Fungi isolated from Otitis Media. Res J Biotechnol. 2024 Sep 30;19(11):192–8.

12. Albandar I, Jabbar S, Ibrahim T, Radhi O, Mbalaha Z. Advances of Nanotechnology in Eradication Bacterial Infectious Diseases: A Recent Review. Kirkuk Journal of Science. 2024 Jun 1;19(2):34–46.

13. Shihab Hamad S, Mohammed Abdullah H. Screening for Toxoplasma gondii antibodies among cancer patients in Kirkuk province by using some serological tests. Kirkuk University Journal-Scientific Studies. 2017 Mar 28;12(1):58–68.

14. Kasim Al-Aubaidi I, Ali Al-Oqaily M, Shahab Hamad S. Role of Interleukin 33 During Infection with Toxoplasmosis in Rheumatoid Arthritis Patients. 526 Indian Journal of Forensic Medicine & Toxicology. 14(1).

15. Aslam R, Mobin M, Shoeb M, Aslam J. Novel ZrO2-glycine nanocomposite as eco-friendly high temperature corrosion inhibitor for mild steel in hydrochloric acid solution. Sci Rep. 2022 Dec 1;12(1).

16. Boran F, Okutan M. Synthesis optimization of ZrO2 nanostructures for photocatalytic applications. Turk J Chem. 2023;47(2):448–64.

17. Chitoria AK, Mir A, Shah MA. A review of ZrO2 nanoparticles applications and recent advancements. Vol. 49, Ceramics International. Elsevier Ltd; 2023. p. 32343–58.

18. Szczyglewska P, Feliczak-Guzik A, Nowak I. Nanotechnology–General Aspects: A Chemical Reduction Approach to the Synthesis of Nanoparticles. Molecules. 2023 Jun 22;28(13):4932.

19. Altammar KA. A review on nanoparticles: characteristics, synthesis, applications, and challenges. Vol. 14, Frontiers in Microbiology. Frontiers Media S.A.; 2023.

20. Begum SJP, Pratibha S, Rawat JM, Venugopal D, Sahu P, Gowda A, et al. Recent Advances in Green Synthesis, Characterization, and Applications of Bioactive Metallic Nanoparticles. Vol. 15, Pharmaceuticals. MDPI; 2022.

21. Dikshit PK, Kumar J, Das AK, Sadhu S, Sharma S, Singh S, et al. Green synthesis of metallic nanoparticles: Applications and limitations. Vol. 11, Catalysts. MDPI; 2021.

22. Khan F, Shariq M, Asif M, Siddiqui MA, Malan P, Ahmad F. Green Nanotechnology: Plant-Mediated Nanoparticle Synthesis and Application. Vol. 12, Nanomaterials. MDPI; 2022.

23. Khalid A, Algarni AS, Homeida HE, Sultana S, Javed SA, Rehman Z ur, et al. Phytochemical, Cytotoxic, and Antimicrobial Evaluation of Tribulus terrestris L., Typha domingensis Pers., and Ricinus communis L.: Scientific Evidences for Folkloric Uses. Evidence-Based Complementary and Alternative Medicine. 2022 Jan 27;2022:1–11.

24. Ghanbari A, Akhshi N, Nedaei SE, Mollica A, Aneva IY, Qi Y, et al. Tribulus terrestris and female reproductive system health: A comprehensive review. Phytomedicine. 2021 Apr 1;84.

25. Ștefănescu R, Tero-Vescan A, Negroiu A, Aurică E, Vari CE. A comprehensive review of the phytochemical, pharmacological, and toxicological properties of tribulus terrestris l. Vol. 10, Biomolecules. MDPI AG; 2020.

26. Abdulqawi LNA, Quadri SA. Evaluation of Antibacterial and Antioxidant activities of Tribulus terrestris L. Fruits. Res J Pharm Technol. 2021 Jan 1;14(1):331–6.

27. Abbas M, Hussain M, Akhtar S, Ismail T, Qamar M, Shafiq Z, et al. Bioactive Compounds, Antioxidant, Anti-Inflammatory, Anti-Cancer, and Toxicity Assessment of Tribulus terrestris—In Vitro and In Vivo Studies. Antioxidants. 2022 Jun 13;11(6):1160.

28. Shakir MM, Sh Hamad S. Scolicidal Potential of Tribulus terrestris L. Aqueous Fruit Extract: An In Vitro Study on Echinococcus granulosus Protoscolices [Internet]. Vol. 11, International Journal of Environmental Sciences. Available from: https://www.theaspd.com/ijes.php

29. Adnan A, Al-Mussawi[2]abbas AAM, Bashi[3] M. Scolicidal Effects of Silver-Copper (core-shell) Nanoparticles Against Echinococcus granulosus Protoscolices in vitro [Internet]. Vol. 25. 2021. Available from: http://annalsofrscb.ro

30. Napooni S, Arbabi M, Delavari M, Hooshyar H, Rasti S. Lethal effects of gold nanoparticles on protoscolices of hydatid cyst: in vitro study. Comp Clin Path. 2019 Feb 5;28(1):143–50.

31. Shnawa BH, Hamad SM, Barzinjy AA, Kareem PA, Ahmed MH. Scolicidal activity of biosynthesized zinc oxide nanoparticles by Mentha longifolia L. leaves against Echinococcus granulosus protoscolices. Emergent Mater. 2022 Jun 1;5(3):683–93.

32. Bouaziz S, Amri M, Taibi N, Zeghir-Bouteldja R, Benkhaled A, Mezioug D, et al. Protoscolicidal activity of Atriplex halimus leaves extract against Echinococcus granulosus protoscoleces. Exp Parasitol. 2021 Oct 1;229.

33. Qanash H, Bazaid AS, Aldarhami A, Alharbi B, Almashjary MN, Hazzazi MS, et al. Phytochemical Characterization and Efficacy of Artemisia judaica Extract Loaded Chitosan Nanoparticles as Inhibitors of Cancer Proliferation and Microbial Growth. Polymers (Basel). 2023 Jan 1;15(2).

34. Liga S, Paul C, Péter F. Flavonoids: Overview of Biosynthesis, Biological Activity, and Current Extraction Techniques. Vol. 12, Plants. Multidisciplinary Digital Publishing Institute (MDPI); 2023.

35. Yu M, Gouvinhas I, Rocha J, Barros AIRNA. Phytochemical and antioxidant analysis of medicinal and food plants towards bioactive food and pharmaceutical resources. Sci Rep. 2021 Dec 1;11(1).

36. Kazi S, Nirwan S, Kunde S, Jadhav S, Rai M, Kamble D, et al. Green Synthesis, Characterization and Bio-evaluation of Zirconium Nanoparticles Using the Dried Biomass of Sphagneticola trilobata Plant Leaf. Bionanoscience. 2022 Sep 1;12(3):731–40.

37. Veerabhadraswamy BN, Pradeep HK, Swaroop K, Manoj KM, Dhanush Nadigar M V, Akash Patel MP, et al. Green synthesis and characterization of Zirconium Oxide with antimicrobial activities. IOP Conf Ser Mater Sci Eng. 2024 Apr 1;1300(1):012036.

38. Chowdhury MA, Hossain N, Mostofa MG, Mia MR, Tushar M, Rana MM, et al. Green synthesis and characterization of zirconium nanoparticlefor dental implant applications. Heliyon. 2023 Jan 1;9(1).

39. Tran T Van, Nguyen DTC, Kumar PS, Din ATM, Jalil AA, Vo DVN. Green synthesis of ZrO2 nanoparticles and nanocomposites for biomedical and environmental applications: a review. Vol. 20, Environmental Chemistry Letters. Springer Science and Business Media Deutschland GmbH; 2022. p. 1309–31.

40. Semerdjieva IB, Zheljazkov VD. Chemical Constituents, Biological Properties, and Uses of Tribulus terrestris: A Review. Nat Prod Commun. 2019;14(8).

41. Gunarathne R, Nadeeshani H, Lu A, Li J, Zhang B, Ying T, et al. Potential Nutraceutical Use of *Tribulus terrestris* L. in Human Health. Food Reviews International. 2023 Sep 8;39(8):5326–55.

42. Malik MY, Alex A, Sivalingam AM, Neha B, Vimal S. Evaluation of the Phytochemical Screening of Methanolic Seed Extracts of Tribulus terrestris: An In Vitro Application of Anti-cancer, Anti-oxidant, and Anti-microbial Activities. Cureus. 2024 Aug 12;

43. Vinay CM, Mehta CH, Bhat C, Kamath A, B Joshi M, Paul B, et al. Integrated LC-MS/MS and network pharmacology approach for predictingactive ingredients and pharmacological mechanisms of *Tribulus terrestris* L. against cardiac diseases. J Biomol Struct Dyn. 2023 Dec 29;41(21):11930–45.

44. Xu X, Guo W, Zhao L, Sun Y, Xu D, Yang J, et al. Exploring the in vitro anti-inflammatory activity of gross saponins of *Tribulus terrestris* L. fruit by using liquid chromatography-mass spectrometry-based cell metabolomics approach. J Sep Sci. 2023 Dec 7;46(24).

45. Tkachenko K, Frontasyeva M, Vasilev A, Avramov L, Shi L. Major and Trace Element Content of Tribulus terrestris L. Wildlife Plants. Plants. 2020 Dec 13;9(12):1764.

46. Yang M, Oppong MB, Di J, Yuan Q, Chang Y, Jiang M, et al. Steroidal saponins with anti-inflammatory activity from Tribulus terrestris L. Acupuncture and Herbal Medicine. 2022 Mar;2(1):41–8.

47. Zhao J, Tian XC, Zhang JQ, Li TT, Qiao S, Jiang SL. Tribulus terrestris L. induces cell apoptosis of breast cancer by regulating sphingolipid metabolism signaling pathways. Phytomedicine. 2023 Nov;120:155014.

48. Oshadie G, Silva D, Abeysundara AT, Minoli M, Aponso W. Extraction methods, qualitative and quantitative techniques for screening of phytochemicals from plants. ~ 29 ~ American Journal of Essential Oils and Natural Products. 2017;5(2):29–32.

49. Bumajdad A, Nazeer AA, Al Sagheer F, Nahar S, Zaki MI. Controlled Synthesis of ZrO2 Nanoparticles with Tailored Size, Morphology and Crystal Phases via Organic/Inorganic Hybrid Films. Sci Rep. 2018 Dec 1;8(1).

50. Horti NC, Kamatagi MD, Nataraj SK, Wari MN, Inamdar SR. Structural and optical properties of zirconium oxide (ZrO2) nanoparticles: Effect of calcination temperature. Nano Express. 2020 Jun 1;1(1).

51. Soltys L, Olkhovyy O, Tatarchuk T, Naushad M. Green synthesis of metal and metal oxide nanoparticles: Principles of green chemistry and raw materials. Vol. 7, Magnetochemistry. MDPI; 2021.

52. Chopra H, Bibi S, Singh I, Hasan MM, Khan MS, Yousafi Q, et al. Green Metallic Nanoparticles: Biosynthesis to Applications. Vol. 10, Frontiers in Bioengineering and Biotechnology. Frontiers Media S.A.; 2022.

53. Kavaz D, Umar H, Aliyu MR. Green Synthesized Metallic Oxide Nanomaterials for Diverse Applications. Vol. 8, NanoWorld Journal. United Scientific Group; 2022. p. 14–22.

54. Agbaje L, Elegbede JA, Akinola PO, Ajayi VA. Biomedical Applications of Green Synthesized-Metallic Nanoparticles: A Review. Pan African Journal of Life Sciences. 2019 Nov 1;3(1):157–82.

55. Napooni S, Delavari M, Arbabi M, Barkheh H, Rasti S, Hooshyar H, et al. Scolicidal Effects of Chitosan–Curcumin Nanoparticles on the Hydatid Cyst Protoscolices. Acta Parasitol. 2019 Jun 1;64(2):367–75.

56. Norouzi R, Ataei A, Hejazy M, Noreddin A, Zowalaty ME El. Scolicidal effects of nanoparticles against hydatid cyst protoscolices in vitro. Int J Nanomedicine. 2020;15:1095–100.

57. Norouzi R, Hejazy M, Ataei A. Scolicidal effect of zinc oxide nanoparticles against hydatid cyst protoscolices in vitro. Nanomedicine Research Journal. 2019;4(1):23–8.

58. Daniel AI, Onogwu SU, Gara TY, Oladunni A, Tijani JO, Oselusi SO, et al. Green-synthesis of MgO and ZrO2 nanocomposites: physicochemical properties and antiplasmodial activity in a mouse model. Discover Applied Sciences. 2025 Apr 23;7(5):382.

59. Goudarzi MG, Bagherzadeh M, Taheri F, Rostami-Vartooni A. Preparation and characterization of magnetic zirconium oxide nanocomposite as a catalyst for reduction of methylene blue. SN Appl Sci. 2020 Jul 1;2(7).

60. Sahani R, Jaybhaye S. Biosynthesis Of Zirconia (ZrO 2) Nanoparticles Using Plant Extract: A Review [Internet]. Vol. 11, International Journal of Creative Research Thoughts (IJCRT) www.ijcrt.org. 2023. Available from: www.ijcrt.org

61. Hamad S, Al-Haidary BAH, Abed ZAS. Effects of Two Genotypes of Toxoplasma gondii Strains on DNA Sequence of Females' Oocytes with Polycystic Ovarian Syndrome. Ann Trop Med Public Health. 2020;23(13).

62. Rahman K, Khan SU, Fahad S, Chang MX, Abbas A, Khan WU, et al. Nano-biotechnology: A new approach to treat and prevent malaria. Vol. 14, International Journal of Nanomedicine. Dove Medical Press Ltd.; 2019. p. 1401–10.

63. Ramesh M, Janani R, Deepa C, Rajeshkumar L. Nanotechnology-Enabled Biosensors: A Review of Fundamentals, Design Principles, Materials, and Applications. Vol. 13, Biosensors. MDPI; 2023.

64. Tiwari R, Gupta RP, Singh VK, Kumar A, Rajneesh N, Madhukar P, et al. Nanotechnology-Based Strategies in Parasitic Disease Management: From Prevention to Diagnosis and Treatment. Vol. 8, ACS Omega. American Chemical Society; 2023. p. 42014–27.

65. Lal M, Sutradhar D. A comprehensive analysis of phytochemicals, antioxidant, anti-inflammatory, antibacterial, antifungal and phytoestrogenic properties of different parts of *Tribulus terrestris*. Nat Prod Res. 2024 Nov 5;17.